# Past warm climate conditions show a shift in Northern Hemisphere winter variability towards a dominant North Pacific Oscillation

Arthur M. Oldeman[1], Michiel L.J. Baatsen[1], Anna S. von der Heydt[1,2], Aarnout J. van Delden[1], and Henk A. Dijkstra[1,2]

[1]Institute for Marine and Atmospheric research Utrecht (IMAU), Department of Physics, Utrecht University, 3584 CC Utrecht, the Netherlands

[2]Centre for Complex Systems Studies, Utrecht University, 3584 CE Utrecht, the Netherlands

**Correspondence:** Arthur Oldeman (a.m.oldeman@uu.nl)

**Abstract.** In this study, we address the question whether the mid-Pliocene climate can act as an analog for a future warm climate with elevated $CO_2$ concentrations, specifically regarding Northern Hemisphere winter variability. We use a set of sensitivity experiments with the global coupled climate model CESM1.0.5, that is a part of PlioMIP2, to separate the response to a $CO_2$ doubling and to mid-Pliocene boundary conditions other than $CO_2$. In the $CO_2$ doubling experiment, the Aleutian low deepens, and the Pacific-North American pattern (PNA) strengthens. In response to the mid-Pliocene boundary conditions, sea-level pressure variance decreases over the North Pacific, the PNA becomes weaker, and the North Pacific Oscillation (NPO) becomes the dominant mode of variability. The mid-Pliocene simulation shows a weak North Pacific jet stream that is less variable in intensity, but has a high level of variation in jet latitude, consistent with a dominant NPO, and indicating that North Pacific atmospheric dynamics become more North Atlantic-like. We show that the weakening of the Aleutian low, and subsequent relative dominance of the NPO over the PNA, is related to the mean surface temperature field in the mid-Pliocene. Variability in the North Atlantic shows little variation between all simulations. The differences between the mid-Pliocene and pre-industrial surface temperature fields are likely caused by differences in orography, which includes the closure of Arctic gateways, rather than a reduced Greenland Ice Sheet. The opposite response in North Pacific winter variability to elevated $CO_2$ or mid-Pliocene boundary conditions demonstrate that the mid-Pliocene climate cannot serve as a future analog in this regard.

## 1 Introduction

Our present climate is warming due to humans increasing the concentration of greenhouse gases in the atmosphere, and there is a need to make accurate projections of our future climate. Future climate is dependent on the emission pathway we choose, and determined by the response of the climate system itself to increased $CO_2$, through feedbacks and natural variations.

A feature where future climate projections fail to give a consistent response to increasing $CO_2$ levels is atmospheric variability in the Northern Hemisphere winter, specifically the Northern Annular Mode (NAM) and its regional expression, the North Atlantic Oscillation (NAO). These modes represent an oscillation of mass between the subpolar latitudes and subtropics in the Northern Hemisphere, and are the leading modes of sea-level pressure (SLP) variability in the northern extratropics (Ambaum et al., 2001; Hurrell and Deser, 2010). The NAO plays a significant role in North Atlantic and European climate, for example

in extratropical storm tracks, and affects projections of temperature and precipitation on an interannual to decadal time scale (Deser et al., 2017; Iles and Hegerl, 2017). Uncertainties in climate projections over the Euro-Atlantic sector are largely related to atmospheric circulation variability (Woollings, 2010; Shepherd, 2014; Fereday et al., 2018), in particular because there is no consensus on how the NAM and NAO respond to increasing $CO_2$ concentrations (Eyring et al., 2021). This is in part due to the large amplitude of internal variability related to the NAO compared to the amplitude of global warming (Osborn, 2004), as well as a considerable model spread in climate change simulations (Eyring et al., 2021). Though climate models are considered skilful in simulating the spatial features and variance of the present-day and historical NAO (Eyring et al., 2021), CMIP5 and CMIP6 models underestimate NAO variability and North Atlantic jet stream variations on a multi-decadal to centennial time-scale (Blackport and Fyfe, 2022).

The two leading modes of atmospheric winter variability over the North Pacific are the Pacific North-American (PNA) pattern and the North Pacific Oscillation (NPO) or West Pacific teleconnection (Barnston and Livezey, 1987; Linkin and Nigam, 2008). The PNA has a large influence on present-day North Pacific and North American winter climate. Linkin and Nigam (2008) state that the NPO shows a strong connection to Arctic sea ice variability, and Hurwitz et al. (2012) show a strengthened NPO in sensitivity experiments with increased North Pacific sea-surface temperatures (SSTs). Both studies indicate that the NPO might play a larger role in a future warm climate. However, Chen et al. (2018) investigate a large ensemble of CMIP5 simulations and find a stronger PNA under high $CO_2$ forcing, but no consensus on the NPO. They find that CMIP5 models reasonably simulate spatial patterns and interannual variations of the present-day and historical PNA and NPO, but lack the capability to reproduce variations on a decadal timescale.

An issue with investigating the response of climate variability to increasing $CO_2$ in the near-future is that the present-day climate system is not in equilibrium with the mean forcing. However, we can use equilibrium climate simulations to investigate the response of natural climate variations to elevated levels of atmospheric $CO_2$. The geological past climate was in equilibrium with forcing, and saw multiple periods with elevated atmospheric $CO_2$ and temperatures of which there is a reasonable amount of geological evidence and reconstructions (see also Chen et al., 2021, FAQ1.3). The most recent period with similar $CO_2$ concentrations as the present-day was the mid-Pliocene warm period, approximately 3 million years (Ma) ago. It had a similar geography - compared to earlier geological periods - to the present-day. The main differences in the northern higher latitudes are the closure of the Bering Strait and Canadian Arctic Archipelago, a reduced Greenland Ice Sheet (GIS), and changes in vegetation. It is considered the 'best analog' for near-future climate, because it represents an equilibrated climate at current levels of atmospheric $CO_2$ (400 ppm) (Burke et al., 2018).

The mid-Pliocene has been investigated using coupled climate models as part of two phases of the Pliocene Model Intercomparison Project (PlioMIP). The most recent PlioMIP2 employs a time-slice approach in order to compare model simulations and proxy reconstructions in a detailed way. Several model-data comparisons and ensemble investigations have been done in the PlioMIP2, for example concerning mean climate (Haywood et al., 2020), El Niño-Southern Oscillation (ENSO, Oldeman et al., 2021; Pontes et al., 2022), Atlantic Meridional Overturning Circulation (AMOC, Zhang et al., 2020; Weiffenbach et al., 2023), the global hydrological cycle (Han et al., 2021) and Arctic warming (De Nooijer et al., 2020). Some of these studies also show very different climate responses to the forcing changes in the mid-Pliocene compared to near-future projections, for

example a stronger AMOC (Weiffenbach et al., 2023) compared to a weakening of the AMOC in the projected future, as well as strongly reduced ENSO variability (Oldeman et al., 2021), which is not projected for near-future climate.

The question addressed here is: can the mid-Pliocene climate be used to assess the response of present-day Northern Hemisphere winter atmospheric variability, such as the NAO, NAM and PNA, to increased $CO_2$? Earlier work by Hill et al. (2011) shows reduced NAM variability in the Pliocene, which was primarily attributed to the lowering of the Rocky Mountains. Both PlioMIP1 and PlioMIP2 employed a time-slice where the Rocky Mountain uplift had already occurred. De Nooijer et al. (2020) find an Arctic warming of 7.2°C in the PlioMIP2 ensemble, compared to the pre-industrial, and a greater level of Arctic amplification compared to CMIP5 future projections. Menemenlis et al. (2021) investigate extratropical hydroclimate changes in the mid-Pliocene using a version of the CCSM4 model, and find large precipitation changes linked to dynamical shifts in atmospheric rivers. A wintertime stationary wave train in the pre-industrial largely disappears in the mid-Pliocene, resulting in fewer atmospheric rivers over the eastern North Pacific region. They use sensitivity studies to show that changes in ice sheets as well as closed gateways are responsible for these differences, and not an increased level of atmospheric $CO_2$. Earlier, Otto-Bliesner et al. (2017) had already shown the large sensitivity of the mid-Pliocene climate to closure of both the Bering Strait and Canadian Arctic Archipelago, compared to the sensitivity to higher $CO_2$. Burton et al. (2023) use a linear fractionation method to show that $CO_2$ is the most important forcing for global surface temperatures and precipitation in the mid-Pliocene, employing a set of sensitivity studies of a selection of PlioMIP2 model contributions. Regionally, there are large differences though, and especially at high latitudes surface temperatures are more forced by changes in boundary conditions other than $CO_2$.

A difficulty with assessing the variability of past winter atmospheres in models is the comparison with proxy data. There is a lack of reconstructions that are either seasonal, interannual or a proxy for the atmosphere, and the majority of reconstructions from the mid-Pliocene represent SSTs. De Nooijer et al. (2020) present a data-model comparison of PlioMIP2 results with annual mean Arctic temperature reconstructions, as well a limited selection of sea-ice extent reconstructions. Tindall et al. (2022) present an analysis of seasonal temperatures between models and reconstructions, but this is limited to surface temperatures. A Pliocene Arctic sea-ice extent record covering the mid-Pliocene warm period is discussed in Behera et al. (2022), but is based on spring sea-ice cover for one site with geological temporal resolution. A reconstruction of Pliocene westerlies is presented in Abell et al. (2021), but again covers a longer geological timescale and focuses on the intensification of the Northern Hemisphere glaciation (2.73 Ma). Lastly, Hill et al. (2011) compares the NAM in Pliocene model simulations with fossil tree-ring reconstructions that give a measure of interannual variations, but these cover the early Pliocene (4-5 Ma) and not the mid- or late Pliocene.

In this paper we investigate Northern Hemisphere winter variability in pre-industrial and mid-Pliocene simulations within one global climate model, the Community Earth System Model (CESM) version 1.0.5, that is a part of the PlioMIP2 ensemble. Since the equilibrated mid-Pliocene climate saw increased $CO_2$ levels as well as different boundary conditions such as topography, land-ice coverage and vegetation, we will use sensitivity simulations to identify the response to both boundary conditions. Starting from a pre-industrial reference simulation with present-day geography and 280 ppm atmospheric $CO_2$, we will assess the response to a $CO_2$ doubling (560 ppm) with present-day boundary conditions, as well as the response to

mid-Pliocene boundary conditions at pre-industrial $CO_2$ level (280 ppm). Both simulations represent 3°C warmer worlds, but due to different forcings (Baatsen et al., 2022).

In the following section, we explain the model and simulations used, outline our analysis methods, and compare our pre-industrial simulations to results from reanalysis data. In section 3, we present results of mean winter climate as well as SLP winter variability for all sensitivity simulations. We also investigate jet stream variations related to SLP variability in response to the mid-Pliocene boundary conditions. The following section presents a discussion and physical interpretation of the results, as well as our answer to the question of the mid-Pliocene as a future analog. A summary and outlook concludes the paper.

## 2 Methods and data

### 2.1 Model and simulations

#### 2.1.1 Model design and configuration

The model used in this study is one out of seventeen contributions to the model ensemble PlioMIP2. The PlioMIP2 methodology for participating modelling groups is outlined in Haywood et al. (2016). In comparison to PlioMIP1, an enhanced set of boundary conditions is supplied (the PRISM4 reconstruction, see Dowsett et al. (2016)). Next to that, the experimental setup is such that it represents a specific time-slice in the mid-Pliocene, the KM5c interglacial (3.205 Ma), where the orbital configuration was similar as the present day. The provided mid-Pliocene boundary conditions include mid-Pliocene topography and bathymetry, coastlines, land surface properties (i.e. vegetation, soil type, and ice sheet coverage), as well as atmospheric composition. Some important aspects of the mid-Pliocene model geography compared to pre-industrial reference are the closure of the Bering Strait and the Canadian Arctic Archipelago (or Northwest Passage). This makes the Arctic Ocean isolated from the North Pacific ocean, as well as from the Labrador Sea. The GIS is significantly reduced in spatial coverage, covering only part of southeastern Greenland and being reduced in height, affecting topography as well.

The CESM is a fully coupled ocean-atmosphere-land-ice general circulation model. For specific use in paleoclimate modelling, version 1.0.5 is a suitable trade-off between model complexity and computational cost. The model version used here employs the atmosphere module CAM4, which is part of the Community Climate System Model version 4 (CCSM4), and can be considered a CMIP5 generation model. Within the PlioMIP2 ensemble our model is, therefore, referred to as CCSM4-Utr. The atmospheric grid has a horizontal resolution of $\sim 2^\circ$ ($2.5^\circ \times 1.9^\circ$ or $144 \times 96$ grid cells) and 26 vertical levels. Details on the model version, simulations, spin-up and general climate features can be found in Baatsen et al. (2022).

The PlioMIP2 model contributions vary in model complexity, resolution, implementation of the provided boundary conditions, as well as in the set of simulations performed. Each model has performed two core experiments, namely a pre-industrial reference simulation at 280 ppm $CO_2$ and a mid-Pliocene simulation at 400 ppm $CO_2$. Following the PlioMIP2 naming convention, these simulations are referred to $E^{280}$ and $Eoi^{400}$, respectively (the “o" and “i" referring to the implementation of Pliocene orography and ice sheets, and the number referring to the atmospheric $CO_2$ concentration). The CCSM4-Utr has performed an

additional set of sensitivity experiments, employing present-day as well as mid-Pliocene geography, vegetation and ice sheets at different levels of atmospheric $CO_2$, which makes it specifically suitable for this study.

### 2.1.2 Performance within PlioMIP2 ensemble

Within the PlioMIP2, results of the pre-industrial $E^{280}$ and mid-Pliocene $Eoi^{400}$ simulations have been compared both to proxy reconstructions, as well as to other ensemble members. Haywood et al. (2020) show that CCSM4-Utr is one of the best performing models in the PlioMIP2 regarding data-model comparison for each site. De Nooijer et al. (2020) study Arctic warming in the PlioMIP2 ensemble, and find that CCSM4-Utr is one of the best performing models considering the data-model comparison of Arctic temperature anomalies. CCSM4-Utr winter sea-ice extent also matches well with reconstructions, although seasonal sea-ice extent reconstructions are very limited. Tindall et al. (2022) show that a significant model-data bias arises in winter months, due to a potential warm bias in the data and a potential cold bias in the models, but this holds for each PlioMIP2 model.

The CCSM4-Utr mid-Pliocene $Eoi^{400}$ simulations have been included in several PlioMIP2 ensemble studies. Oldeman et al. (2021) show that the mid-Pliocene ENSO variability was reduced compared to the pre-industrial, and that CCSM4-Utr has the most reduced ENSO variability of the ensemble (67% reduction compared to 24% in the ensemble mean). Pontes et al. (2022) also study PlioMIP2 ENSO and find a relation between the reduced ENSO and a northward shift in Pacific ITCZ. They show that CCSM4-Utr exhibits the largest northward shift of the ITCZ from October to February. Zhang et al. (2020) and Weiffenbach et al. (2023) show an increased AMOC strength in the PlioMIP2 ensemble. Weiffenbach et al. (2023) furthermore explain that models with a closed Bering strait and Canadian Arctic Archipelago (including CCSM4-Utr) show reduced freshwater transport from the Arctic Ocean into the North Atlantic, causing an increase in subpolar North Atlantic salinity, which drives the stronger AMOC. In this case, CCSM4-Utr simulates a stronger AMOC in the mid-Pliocene with values close to the ensemble mean (22 Sv over 19 Sv in the pre-industrial).

### 2.1.3 Simulation specifics

The PlioMIP2 naming convention is used for our set of sensitivity simulations. The reference simulation is the pre-industrial $E^{280}$ with present-day boundary conditions (BCs; orography, ice sheets and vegetation) and 280 ppm atmospheric $CO_2$. We perform a $CO_2$ doubling simulation at present-day geography ($E^{560}$) to investigate the effect of radiative forcing alone. We also perform a mid-Pliocene BCs experiment at pre-industrial carbon levels ($Eoi^{280}$), to investigate the response to the mid-Pliocene orography, ice sheets and vegetation, but not to $CO_2$. All simulations have spin-up times of around 3,000 model years, and analysis of the results of the $Eoi^{400}$ simulation is found in Baatsen et al. (2022).

For the sake of consistency, we use pre-industrial and $CO_2$ doubling simulations that employ a 'paleoclimate' vertical ocean diffusivity, that we also use in the mid-Pliocene simulations. The difference between this adapted $E^{280}$ and the $E^{280}$ that is used in most PlioMIP2 studies, as well as the motivation for using a different parametrisation, is discussed in Baatsen et al. (2022). The effect of this parametrisation difference was found to be very minimal on ocean surface temperatures and negligible for atmospheric variables. The $CO_2$ doubling experiment was also rerun with this paleo mixing parametrisation. The $E^{280}$ and $E^{560}$

simulations are spun-up from equilibrated simulations and have spin-up times of 4,000 and 2,500 model years, respectively (details on the spin up can be found in Supplementary Material Figure S1).

### 2.2 Data analysis and methodology

In order to investigate Northern Hemisphere winter climate and variability, we study 200 years per simulation, and we use monthly mean Januaries only. Results for December-January-February (DJF) or climatological winter were found to give very similar results for the sake of this study.

We investigate the mean state, so the mean of all 200 Januaries, as well as variability on top of this mean state. We consider SLP, near-surface air temperature (SAT) and sea-ice extent (SIE), as well as zonal winds and potential vorticity (PV) in the higher troposphere. To identify the subtropical jet stream we investigate zonal wind on the 200 hPa isobar (U200). We also compute the location of the dynamical tropopause, here defined as the isoline of 2 PVU (Potential Vorticity Units) at 200 hPa. We also compute the dynamical tropopause defined as the largest zonal PV gradient per longitude, but it gave very similar results as using the 2PVU isoline. The dynamical tropopause at 200 hPa generally follows the subtropical jet stream core (Kunz et al., 2011). The vertical levels of the model are on a hybrid sigma scheme, so results in the vertical have been interpolated onto pressure levels.

To study winter climate variability we focus on the temporal behaviour of SLP. Before analysis, a Lowess smoothing is applied to each spatial grid point using a 50 year moving window. We also compare with reanalysis data, where the same filtering is applied to remove any trend due to anthropogenic climate change. A window size of 50 years was chosen since we are mainly interested in interannual and decadal winter variability. Furthermore, CMIP5 models are known to underestimate variations of multidecadal periods of the winter NAO and jet stream (Blackport and Fyfe, 2022). We use Empirical Orthogonal Function (EOF) analysis to separate the SLP variance in orthogonal modes of spatial and temporal variability. Spatial EOF patterns as well as their corresponding Principal Component (PC) time series are obtained from the Lowess filtered SLP data using a spatial weighting that corresponds to the cosine of the latitude. The EOF patterns are normalised using their spatial standard deviation.

We perform EOF analysis over the Northern Hemisphere (NHem), as well as over the North Atlantic (NAtl, 90°W - 30°E) and North Pacific (NPac, 120E° - 120°W) basins. The regions were chosen such that they include the centers of action of known present-day modes of climate variability, specifically the NAM, NAO and PNA, but also to be equal in longitudinal width. All regions, including the NHem, are bound in latitude between 20°N and 85°N. In the NAtl and NPac regions, we consider the first and second EOF, that we sort based on their level of zonality. The NAO is essentially the zonal mode in the NAtl (NAtl-z), while the PNA would be the North Pacific azonal mode (NPac-a). We chose this classification because modes such as the NAO are well defined in the present-day climate, but may have a different pattern or prominence in a past climate with different boundary conditions. The EOFs and PCs of the NHem, NAtl-z and NPac-z modes are defined such that the mean EOF in the region north of 75°N is positive, while the NAtl-a and NPac-a modes are defined such that the mean EOF in the region 50-60°N is negative.

We investigate in what way the different modes of winter variability in the whole Northern Hemisphere and over the North Pacific and North Atlantic basins are connected. We quantify the level of correlation by means of the Pearson correlation coefficient between the PCs of the corresponding modes. The correlation coefficient between the zonal and azonal mode in either the North Pacific or North Atlantic will always be zero, since these EOFs are orthogonal by definition.

We also perform an analysis of jet variations in the North Pacific. For variations in the central North Pacific jet stream, we limit ourselves to the 200 hPa level and the zonal mean between 160°E and 220°E (or 140°W). We define jet intensity as the maximum of the zonal wind velocity in this sector, and jet latitude as the latitude corresponding to this maximum. Lastly, we investigate the jet stream in the phases of NPac-z mode, where we define the PLUS phase as the average of the top 5% (or ten Januaries) NPac-z PC values, and the MIN phase as the average of the bottom 5% NPac-z PC values.

### 2.3 Validation of $E^{280}$ with reanalysis data

We compare the pre-industrial $E^{280}$ simulation to 19th and 20th century reanalysis data. It is not be a one-on-one comparison, since our pre-industrial simulation is an equilibrium scenario, while any kind of global reanalysis dataset will be influenced by human-induced climate change trends, and will thus be transient. We use assimilated sea-level pressure date from the NOAA/CIRES/DOE 20th Century Reanalysis version 3 (from here on abbreviated as CR20). The data runs from 1836 to 2015 and is assimilated using surface pressure observations on a 1.0° latitude x 1.0° longitude grid. An evaluation of the performance of the CR20v3 can be found in Slivinski et al. (2021). We interpolate the CR20 data onto the model grid when computing differences between the $E^{280}$ and CR20.

A comparison of mean SLP and the related patterns of variability between our pre-industrial simulation and reanalysis is shown in Figure 1. Mean SLP (MSLP) is shown in Figure 1a. The mean MSLP difference is very small (-0.1 hPa). Differences with the CR20 include an overestimation of the subtropical high pressure regions, specifically over the North Atlantic and North-African region, Central Asia and to a smaller extent over North America (up to +12.8 hPa). A lower MSLP is simulated in the subpolar low pressure region in the North Atlantic (up to -12.4 hPa), and the pattern extends more eastward. The North Pacific subpolar low pressure area, the Aleutian low, is well captured in spatial extent and amplitude. Figure 1b shows SLP standard deviation (SD). SLP SD is generally overestimated in the $E^{280}$ (mean SLP SD difference is +1.6 hPa), especially over the North Pacific and Siberian Arctic (up to +5.5 hPa). SLP SD in the North Atlantic storm track region as well as to the east of the tip of Greenland is slightly underestimated. A higher (lower) modelled SLP variance in the North Pacific (North Atlantic) in comparison to observations is a known bias for most CMIP5 and CMIP6 models (Eyring et al., 2021).

Figures 1c-g show the spatial EOF patterns of SLP in the Northern Hemisphere (NHem), North Pacific (NPac) and North Atlantic (NAtl), including the percentage of variance explained for each mode. The NHem mode in Figure 1c represents the NAM or AO and explains more variance in the $E^{280}$ than in the reanalysis (28.7% over 22.2%). The amplitudes of the North Atlantic centers of action are underestimated in the $E^{280}$, which can be expected since the $E^{280}$ simulated less SLP variance in that region.

The leading mode in the NPac is the azonal mode (NPac-a, Figure 1f), explaining around 42% of SLP variance in both $E^{280}$ and CR20. It represents a mode known as the Pacific-North American pattern (PNA), that essentially captures most of

the variability of the Aleutian low pressure system (Barnston and Livezey, 1987). The second leading mode in the NPac is the zonal mode (NPac-z, Figure 1d), explaining 25% (22%) of SLP variance in the $E^{280}$ (CR20). It is known as the North Pacific Oscillation (NPO) and is strongly linked to meridional modulation of the Asian-Pacific jet and Pacific storm track variability, as well as the position and strength of the Aleutian low (Linkin and Nigam, 2008). The $E^{280}$ simulates the spatial pattern well, although the amplitude of the centers of action are a bit less pronounced and the variance more spread out over the region.

The leading mode in the NAtl is the zonal mode (NAtl-z, Figure 1e), explaining 32% (33%) of SLP variance in the $E^{280}$ (CR20), representing the NAO. The amplitude of the southern node is slightly underestimated, while the northern center of action is shifted towards the east. Again, this can be expected from the differences in total SLP variance as shown in Figure 1b. The second leading mode in the NAtl is the azonal mode (NAtl-a, Figure 1g), explaining 20% (21%) of SLP variance in $E^{280}$ (CR20). It is a mode known as the East Atlantic pattern (EA), that usually has its center of action over the British isles (Barnston and Livezey, 1987). The weak but distinct eastern node with opposite sign in the CR20 disappears in the $E^{280}$, likely because the variance shifts more eastward in $E^{280}$. Furthermore, where the CR20 shows that the sign of variability over Greenland is the same sign as in the center of the monopole, the $E^{280}$ shows a clear opposite sign over Greenland. Again, also for this mode the total SLP variance in this region is underestimated.

In summary, we can say that the $E^{280}$ pre-industrial simulation reproduces the MSLP and SLP variability from the CR20 reanalysis quite well. The modes in the North Pacific are captured well in spatial extent, amplitude as well as percentage of variance explained. The modes in the North Atlantic are well reproduced, albeit less accurate, especially regarding amplitudes. However, this is a likely cause of the fact that total SLP variance in the North Atlantic is reduced, which is a known bias in both CMIP5 and CMIP6 models (Eyring et al., 2021).

## 3 Results

### 3.1 Mean winter climate

#### 3.1.1 Mean sea-level pressure

Figure 2a shows the $E^{280}$ MSLP results for a slightly larger domain than in Figure 1a. The January MSLP difference with $E^{560}$ and $Eoi^{280}$ is shown in Figure 2 b and c, respectively. While the SLP response to $CO_2$ doubling is overall relatively small, the response to mid-Pliocene BCs is significantly larger, especially over the North Pacific. The large increase in MSLP over the North Pacific (+16 hPa) results in a reduced SLP difference between the North Pacific subtropical high and subpolar low pressure areas, as well as a slight poleward shift of the latitude with the largest SLP gradient. MSLP furthermore decreases over the Arctic in the $Eoi^{280}$ (up to -7 hPa). When comparing with the mid-Pliocene reference simulation $Eoi^{400}$ (annual mean in Baatsen et al. (2022), January mean in Supplement Figure S2), we see that the MSLP response is largely caused by the mid-Pliocene boundary conditions, and not by the $CO_2$ increase. Only the MSLP decrease around Greenland and especially over the Baffin Bay and the Labrador Sea is a clear combination of the response to mid-Pliocene BCs and to elevated $CO_2$, as it can be observed both in the $E^{560}$ and $Eoi^{280}$ results.

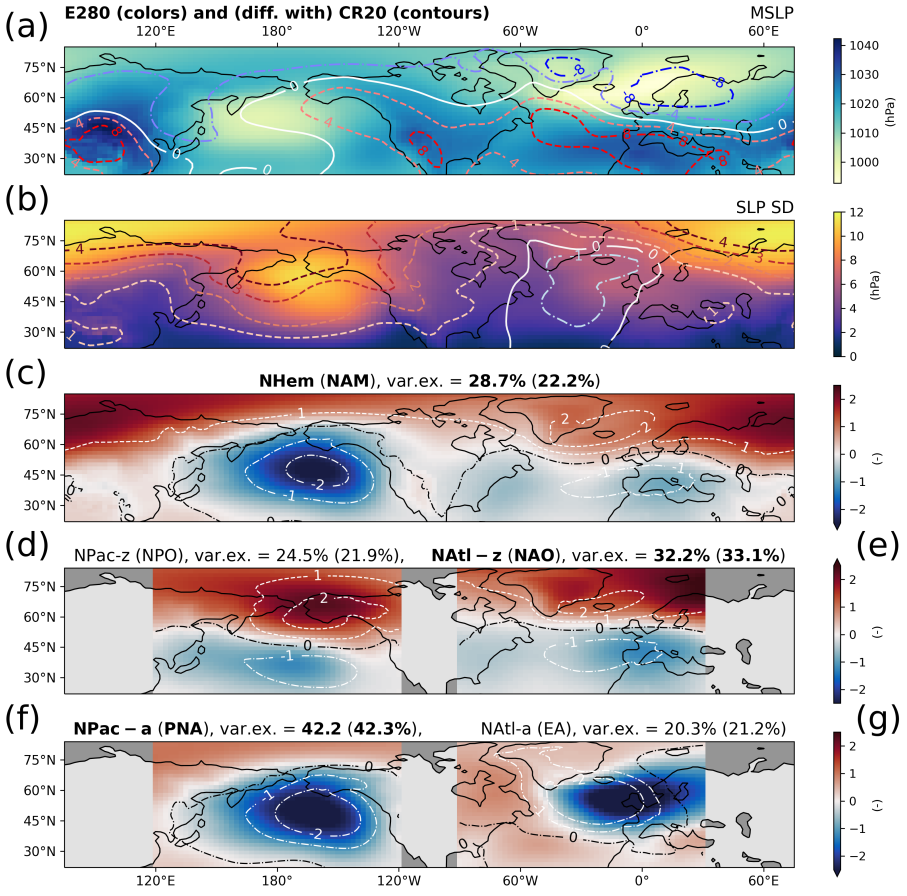


**Figure 1.** Quantification of January sea-level pressure (SLP) variability for $E^{280}$ (colors) and CR20 (contours). (a) Mean sea-level pressure (MSLP), (b) SLP standard deviation (SLP SD), (c) NHem; leading SLP EOF in Northern Hemisphere, (d) NPac-a; zonal SLP EOF in North Pacific, (e) NAtl-z; zonal SLP EOF in North Atlantic, (f) NPac-a; azonal SLP EOF in North Pacific and (g) NAtl-a; azonal SLP EOF in North Atlantic. For (a) and (b), the contours represent the difference between the $E^{280}$ and CR20, while (c)-(g) show the CR20 EOFs in contours. Percentage variance explained by each EOF shown for $E^{280}$, and for CR20 in brackets. In **bold** the (variance of the) leading mode in North Pacific and Atlantic regions.

### 3.1.2 Surface temperatures and sea-ice extent

Figure 3a presents January SAT and SIE for the pre-industrial reference $E^{280}$. Arctic cold spreads far south over the continental regions, specifically Siberia and northern Canada. SAT distributions over land and the ocean, as well as the SIE, are largely as expected from present-day and historical observations.

The SAT difference ($E^{560}$ - $E^{280}$) and SIE for $E^{560}$ show that most continental areas warm slightly more compared to oceans at similar latitudes (Figure 3b). Furthermore, a clear Arctic amplification signal can be observed. This response is expected

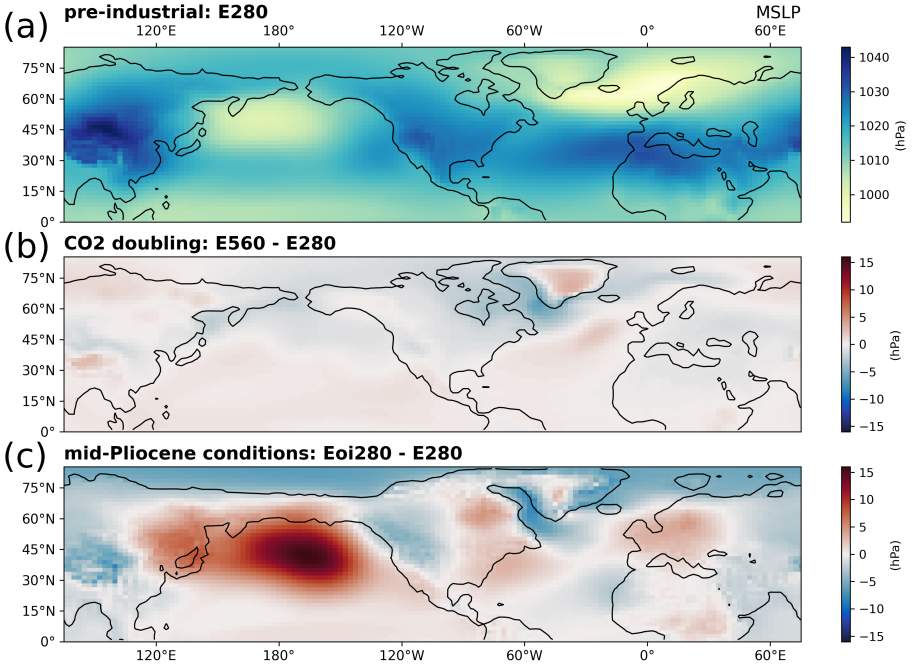


**Figure 2.** January mean sea-level pressure (SLP) results. (a) $E^{280}$, (b) $E^{560}$ min $E^{280}$, (c) $Eoi^{280}$ min $E^{280}$.

with increasing atmospheric $CO_2$ levels. Temperatures increase more than 15°C over the Iceland, Norwegian and Barents Seas, accompanied with a significant poleward retreat of the SIE. Extensive warming is furthermore found in the Labrador Sea, Bering Strait and Okhotsk Sea, all accompanied by sea-ice retreating to higher latitudes.

The SAT response for the $Eoi^{280}$ is in many ways similar to the SAT response for the $CO_2$ doubling (Figure 3c). An Arctic amplification response is present even without any increase in $CO_2$ levels. Again, we see a large warming over the Greenland Sea and Okhotsk Sea, both with poleward retreating SIE. A large SAT increase and SIE retreat is present over the Baffin Bay and Labrador Sea. In the $Eoi^{280}$ results, we see a warmer region over the western and central North Pacific and a large area of cooling over western North America and the land bridge that is now the Bering Strait. This SAT dipole is consistent with the MSLP increase over the North Pacific and decrease over western North America as seen in Figure 2c.

### 3.1.3 Subtropical jet stream and dynamical tropopause

Figure 4a shows $E^{280}$ zonal wind as well as the dynamical tropopause on the 200 hPa isobar. The subtropical jet stream can clearly be identified as a streak of high zonal wind roughly between 25°N and 45°N. The dynamical tropopause generally follows the jet core closely. The jet is strong and concentrated over eastern Asia and the North Pacific Ocean. Over the North Atlantic Ocean, two separated jet streams can be seen, roughly between 20-25°N and 45-50°N. The migration of the subtropical jet towards higher latitudes over the Atlantic, compared to the Pacific, corresponds to the subtropical high and subpolar high being more extended northwards (see Figure 2a).

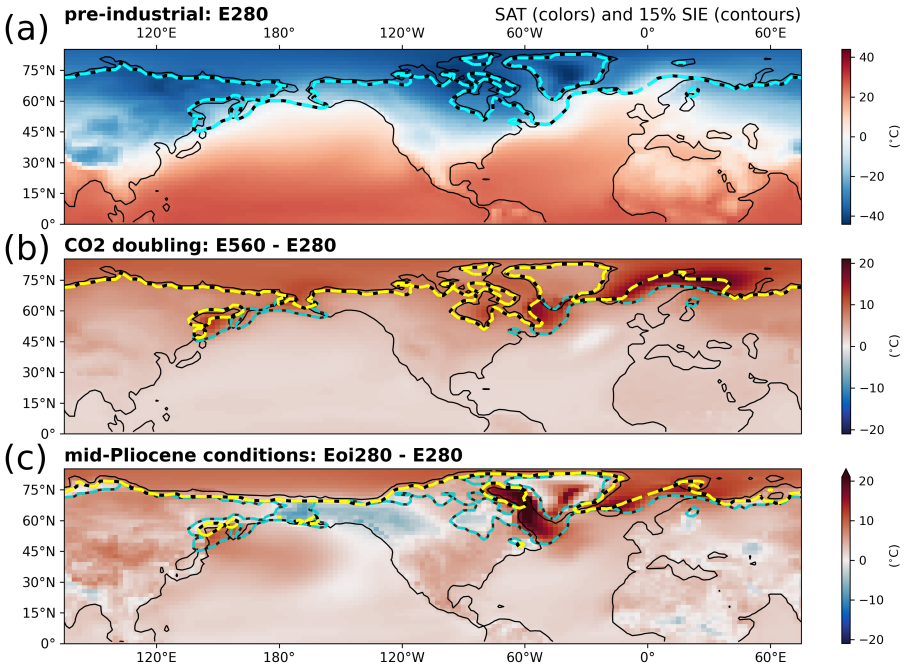


**Figure 3.** January mean surface air temperature (SAT, colors)) and 15% sea-ice extent (SIE, contours) results. (a) $E^{280}$ SAT and SIE (black-blue dashed line), (b) $E^{560}$ min $E^{280}$ SAT (colors) and $E^{560}$ SIE (yellow-black dashed line), (c) $Eoi^{280}$ min $E^{280}$ SAT (colors) and $Eoi^{280}$ SIE (yellow-black dashed line). In (b) and (c), the black-blue dashed line is the $E^{280}$ SIE.

The $E^{560}$ response in zonal wind is very minimal and limits itself to a few meters per second at most (Figure 4b). Over the Pacific, a slight increase in wind speeds is found along the center and southern side of the dynamical tropopause. Over the Euro-Atlantic sector, the response is relatively weak. The largest increase in zonal wind in the Pacific is 4.4 m/s, which is less than the mean time variation of the $E^{280}$ zonal wind (defined as the SD in time, 5.9 m/s).

Generally, the response to the mid-Pliocene conditions (Figure 4c) is a lot stronger compared to the response to $CO_2$ doubling, with the largest response over the North Pacific. The subtropical jet stream weakens significantly over the exit of the East Asian jet and continues to weaken over the whole of the North Pacific, with reductions of up to 25 m/s along the jet core, corresponding to 50% over the central North Pacific. Apart from the reduction in jet strength along 30°N, we also see an increase in zonal wind over the northern North Pacific, which indicates that apart from weakening, the subtropical jet shifts or expands polewards. The weakening and widening of the North Pacific subtropical jet is consistent with the slight reduction in SLP difference between the subtropical high and subpolar low (see Figure 2c). The dynamical tropopause follows the same curve as the pre-industrial over most of the North Americas, Atlantic ocean and Eurasian continent. Over the Atlantic, the zonal wind decreases slightly along the dynamical tropopause, whereas it increases southward of it.

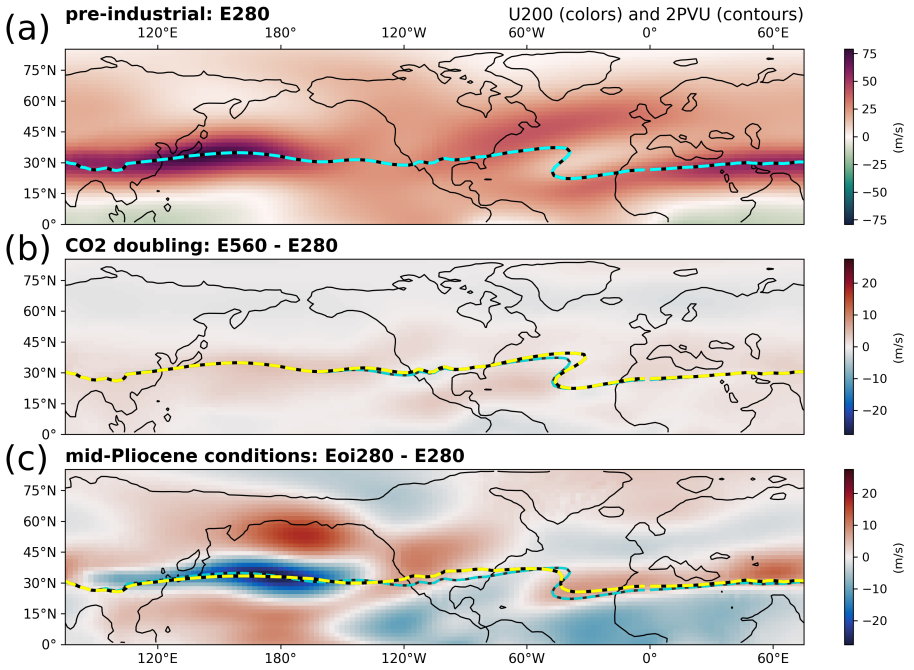


**Figure 4.** January mean zonal wind (U200, colors) and mean of the dynamical tropopause (2PVU, blue-black dashed line) at 200 hPa. (a) $E^{280}$ U200 and 2PVU (black-blue dashed line), (b) $E^{560}$ min $E^{280}$ U200 (colors) and $E^{560}$ 2PVU (yellow-black dashed line), (c) $Eoi^{280}$ min $E^{280}$ U200 (colors) and $Eoi^{280}$ 2PVU (yellow-black dashed line). In (b) and (c), the black-blue dashed line is the $E^{280}$ 2PVU.

### 3.2 Sea-level pressure variability

Following the large changes in mean winter climate of the mid-Pliocene conditions sensitivity experiment, we will now analyse the changes in atmospheric variability by means of EOF analysis of the SLP in the Northern Hemisphere (NHem), North Pacific (NPac) and North Atlantic (NAtl) sectors.

#### 3.2.1 $CO_2$ doubling

Figure 5a shows the $E^{560}$ SLP SD and SLP SD difference with $E^{280}$ in contours. In most of the Northern Hemisphere, there are no notable changes in SLP SD. Only in the center-east North Pacific, there is an increase in SLP SD in the $CO_2$ doubling simulation with regards to the pre-industrial.

The spatial pattern as well as regional amplitude of the NHem mode and the zonal and azonal modes in the NPac and NAtl are very similar in the $E^{560}$ and $E^{280}$ (Figures 5b-f). As in the pre-industrial, the leading mode in the Pacific (Atlantic) is the azonal (zonal) mode. In the NHem EOF, the amplitude of the North Pacific center of action is slightly increased, while the amplitude of the North Atlantic-Siberian center of action is reduced. The NHem mode explains more of the total SLP variance

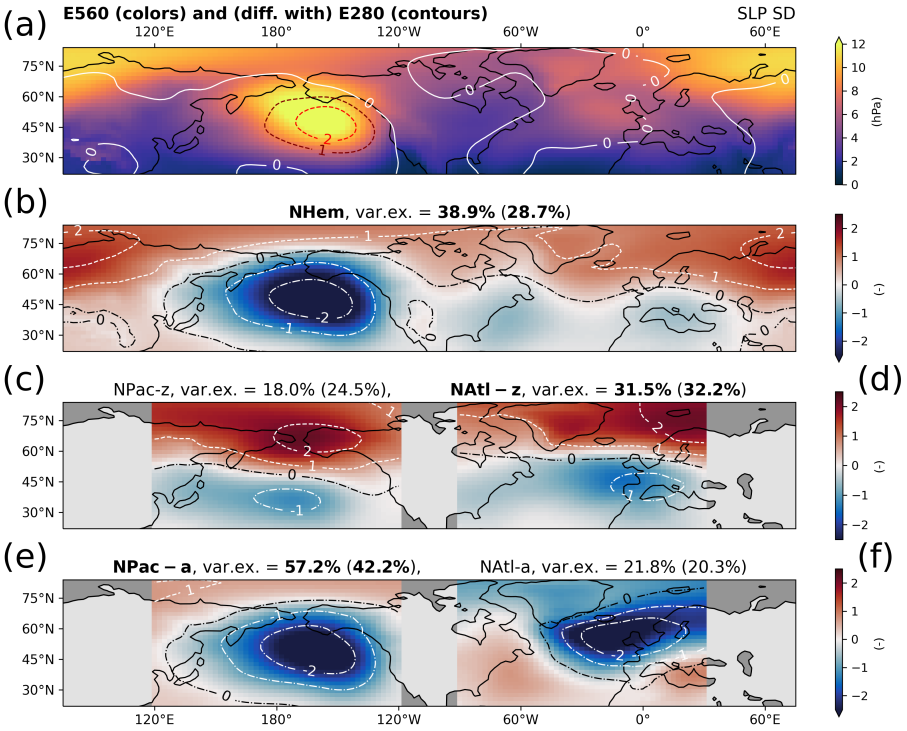


**Figure 5.** January SLP variability in $CO_2$ doubling ($E^{560}$; colors) and pre-industrial ($E^{280}$; contours) experiments. (a) $E^{560}$ SLP standard deviation (SD, colors) and $E^{560}$ min $E^{280}$ SLP SD (lines), (b) leading SLP EOF in Northern Hemisphere, (c) zonal SLP EOF in North Pacific, (d) zonal SLP EOF in North Atlantic, (e) azonal SLP EOF in North Pacific and (f) azonal SLP EOF in North Atlantic. Percentage variance explained by each EOF shown for $E^{560}$, and for $E^{280}$ in brackets. In **bold** the leading mode in North Pacific and Atlantic regions.

in the $CO_2$ doubling (38.9%) compared to the pre-industrial (28.7%). Both results are consistent with the fact that there is simply more SLP variance over the North Pacific (variance defined as square of the SLP SD, Figure 5a).

The two leading modes in the NPac explain more SLP variance in the $CO_2$ doubling experiment compared to the pre-industrial (75.2% over 66.7%, Figures 5c and e). This is mainly because the leading NPac-a mode becomes more dominant, explaining 57.2% of the total SLP variance in this region, which is a lot more compared to the $E^{280}$ (42.2%). The second leading NPac-z mode explains a bit less of the total SLP variance. The two leading modes in the NAtl are shown in Figures 5d and f and the percentage of variance explained remains the same in the $E^{280}$ and $E^{560}$. The dipole of the leading NAtl-z mode is shifted slightly polewards, and the southern node is shifted slightly westward. For the NAtl-a mode, the separation between positive and negative amplitude (or red and blue) moves over the Canadian archipelago in the $E^{560}$, while it moves eastward and poleward from the southern tip of Greenland in the $E^{280}$.

### 3.2.2 Mid-Pliocene boundary conditions

Figure 6a shows the $Eoi^{280}$ SLP SD and SLP SD difference with $E^{280}$ in contours. In general, there is a decrease in SLP SD in the mid-Pliocene experiment. However, there is a substantive decrease in SLP SD over the northeastern North Pacific, while there is a small increase in SLP SD over the Canadian Arctic. Furthermore, there is a decrease in SLP SD over the Scandinavian Arctic and eastern Siberia. No large changes are observed over the Atlantic. The changes in SLP SD in the $Eoi^{280}$ are very similar to the SLP SD changes in the $Eoi^{400}$ (see Supplementary Material Figure S2).

The spatial patterns of the NHem mode and zonal and azonal modes in the NPac and NAtl are similar for the $Eoi^{280}$ and $E^{280}$ (Figures 6b-f). Still, some distinct differences can be seen. The leading mode in the NAtl is still the zonal mode, but the leading mode in the NPac becomes the zonal mode, whereas it is the azonal mode in the $E^{280}$. The spatial pattern of the NHem mode over the North Pacific changes quite drastically, describing more of a dipole rather than a large single center of action. The NHem mode thus becomes more zonal or annular. The percentage of SLP variance explained is similar in the $Eoi^{280}$ (28.3%) compared to the $E^{280}$ (28.7%).

The two leading modes in the NPac together explain slightly less of the total SLP variance in comparison to the pre-industrial (63.9% over 66.7%, Figures 6c and e). The leading mode becomes the zonal mode, explaining almost double the variance that it explains in the $E^{280}$ (45.5% over 24.5%). The spatial pattern is very similar, but differences are that the whole dipole is shifted slightly polewards, and that both centers of action are more spread out spatially, thus representing SLP variations over a larger area. The second leading mode in the NPac becomes the azonal mode, explaining only 18.4% of the SLP variance compared to 42.2% in the pre-industrial. The spatial extent of the monopole is slightly shifted polewards, and the region with largest amplitude extents more over the northwestern North American continent. The dominance of the NPac-z over the NPac-a is consistent with the change in SLP variance (or squared SLP SD) over this region (Figure 6a).

The leading mode is the NAtl-z (Figures 6d) and explains almost the same amount of SLP variance (32.7% over 32.2%). The centers of action of the dipole are shifted slightly polewards. Especially the southern node is more centred over northwestern European mainland, while the northern node is retreated polewards and weakened. The NAtl-a (Figures 6f) explains slightly less variance in the $Eoi^{280}$ (17.5% over 20.3%). The center of action is shifted polewards and spread out further towards the northeast. The southern separation between negative and positive amplitude is shifted northwards over the European mainland. Over the western part of the sector, the mode resembles a dipole with a strong northern node and weak southern node.

### 3.2.3 Correlations between modes

Figure 7a presents the PC correlation matrix for the $E^{280}$ as well as the CR20 reanalysis. The correlations are very similar in both cases, as can be observed from the high level of symmetry with respect to the diagonal. Both show a strong correlation between the NHem and the NAtl-z and NPac-a modes. However, in the CR20 reanalysis these correlations are of similar magnitude while the $E^{280}$ shows a much stronger correlation with the NPac-a than the NAtl-z. This is consistent with the lower (higher) SLP variance over the North Atlantic (North Pacific) in the $E^{280}$ compared to the CR20 as shown in Figure 1b.

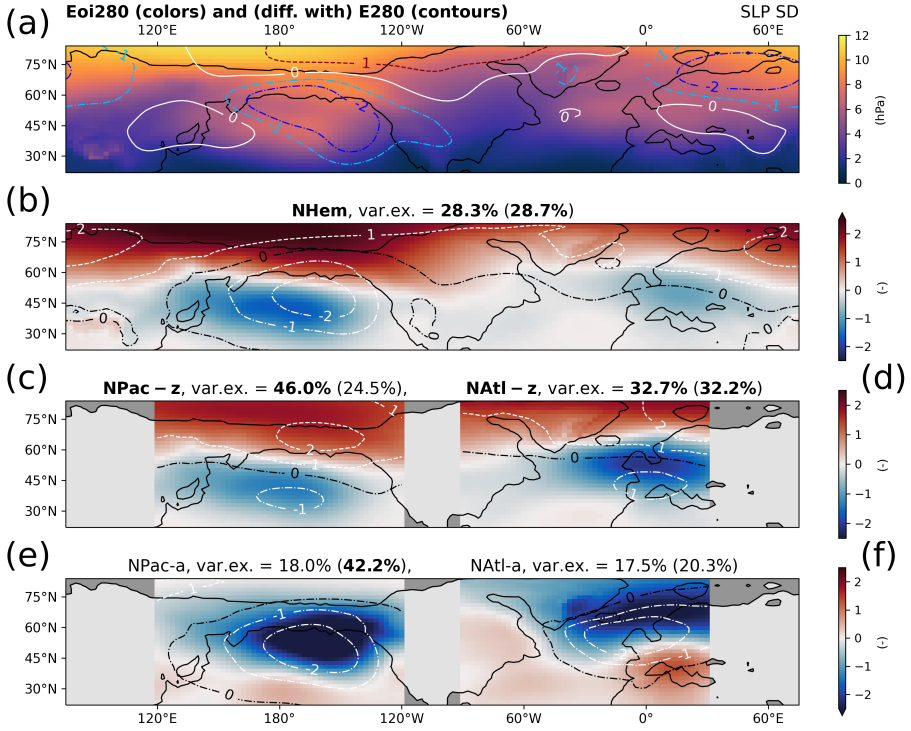


**Figure 6.** January SLP variability in mid-Pliocene conditions (Eoi$^{280}$; colors) and pre-industrial (E$^{280}$; contours) experiments. (a) Eoi$^{280}$ SLP standard deviation (SD, colors) and Eoi$^{280}$ min E$^{280}$ SLP SD (lines), (b) leading SLP EOF in Northern Hemisphere, (c) zonal SLP EOF in North Pacific, (d) zonal SLP EOF in North Atlantic, (e) azonal SLP EOF in North Pacific and (f) azonal SLP EOF in North Atlantic. Percentage variance explained by each EOF shown for E$^{560}$, and for E$^{280}$ in brackets. In **bold** the leading mode in North Pacific and Atlantic regions.

The strongest correlation between basins is between the NPac-a and NAtl-z, which can be expected since both are strongly correlated with the NHem. The NPac-z does not correlate strongly with any other mode in both the E$^{280}$ and CR20.

The correlation matrix for the E$^{560}$ shown in Figure 7b shows great similarities with the E$^{280}$. However, a notable difference is the even stronger correlation between the NHem and NPac-a of 0.98, that is consistent with the increase in SLP variance explained by the NPac-a mode in the E$^{560}$ (see Figure 5e). Interestingly, the NHem mode is more strongly (anti)correlated with the NAtl-a than the NAtl-z, which is not very obvious based on the similarities of the spatial patterns only. The NHem mode shows the strongest correlation with both azonal modes, and simultaneously both azonal modes in the North Pacific and North Atlantic show a stronger correlation. Again, the NPac-z does not strongly correlate with another mode.

The Eoi$^{280}$ correlation matrix shown in Figure 7c shows some notable differences with respect to the E$^{280}$ and E$^{560}$. The correlation between the NHem and NPac-a almost completely disappears. The correlation between the NHem and NPac-z is 0.95 in the Eoi$^{280}$, while being very small in the other simulations. The NHem mode shows the strongest correlation with both zonal modes, agreeing with the earlier result that it represents a more annular mode. There is not a very strong correlation

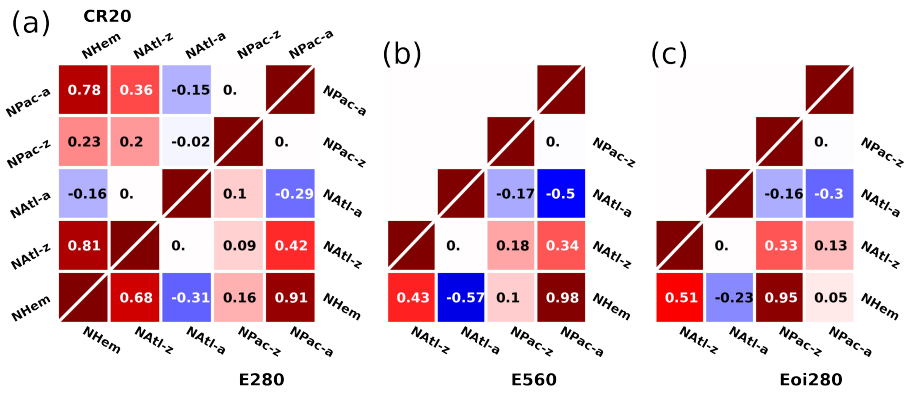


**Figure 7.** Correlation coefficients between Principal Components (PCs) corresponding to EOFs of NHem, NAtl zonal and azonal, NPac zonal and azonal modes of variability. For CR20 (a, top left), $E^{280}$ (a, bottom right), $E^{560}$ (b) and $Eoi^{280}$ (c).

between both zonal modes, however, as well between both azonal modes. In the $Eoi^{280}$, the NPac-a becomes the mode that does not correlate strongly with any other mode.

### 3.3 North Pacific variability and the jet stream

In this section, we focus on the $Eoi^{280}$ and $E^{280}$ results and investigate the impact of the changes in SLP variability on the jet stream in the North Pacific.

#### 3.3.1 SLP variability and jet variations in the central North Pacific

The temporal behaviour of the $E^{280}$ and $Eoi^{280}$ central North Pacific jet stream is shown in Figure 8a and b, by means of a Hovmöller diagram of the zonal mean zonal wind at 200 hPa averaged over 160°E - 220°E. The $E^{280}$ shows a strong and focused jet with little latitudinal variations. On the other hand, the $Eoi^{280}$ shows a generally weaker jet with a great latitudinal variation.

The jet intensity, as well as jet latitude, versus the PC of the NPac-a and NPac-z modes, respectively, are shown in Figure 8c and d. Figure 8c shows that the $E^{280}$ jet intensity correlates strongly and significantly (corr. coeff. of 0.92) with the NPac-a mode. Interestingly, the $Eoi^{280}$ jet shows the same strong and significant correlation (corr. coeff. of 0.92), but with a distribution of much lower wind speeds, and much smaller $R^2$. This means that in both simulations, the jet intensity is linked to the phase of the NPac-a mode.

Figure 8d shows the relation between the jet latitude and the PC of the NPac-z mode. In both simulations, a clear anticorrelation between the jet latitude and the NPac-z mode is apparent. In the $E^{280}$, the jet is located between 30-40°N. In the $Eoi^{280}$, the jet latitude covers a much larger range, and the histogram reveals a less unimodal distribution, with two weak peaks at 30-40°N and 45-55°N. The scatter plot shows that at negative NPac-z PC values, in most years the max zonal wind is found at higher latitudes, but in some Januaries the jet latitude is found between 20-30°N. It suggests the existence of a state with two jets,

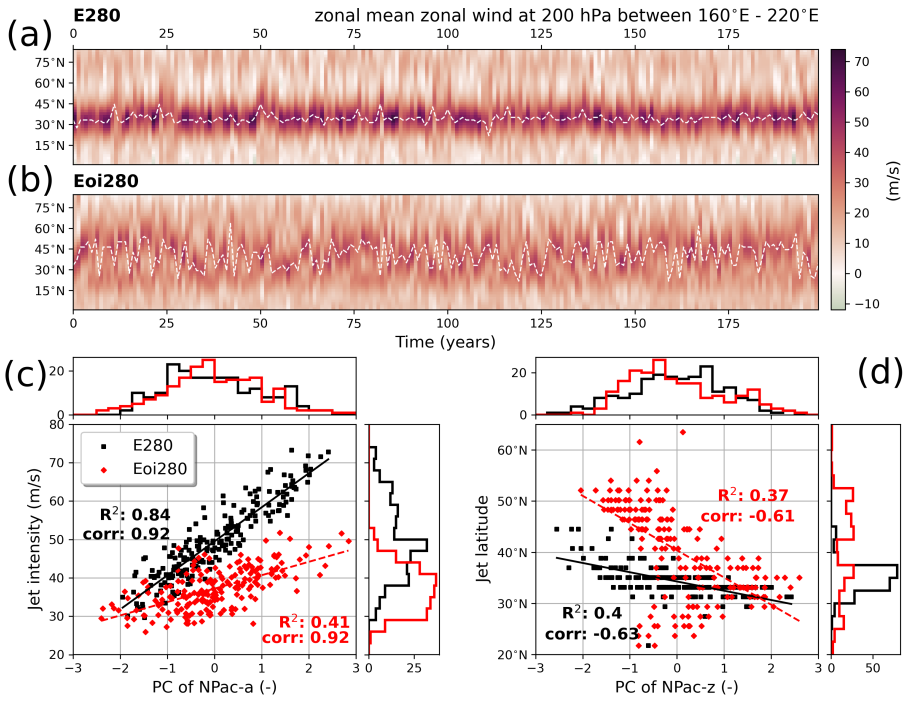


**Figure 8.** (a,b) Hovmöller diagrams showing zonal mean zonal wind at 200 hPa in the 160°E - 220°E mean for every January for the $E^{280}$ (a) and $Eoi^{280}$ (b). The white dashed line follows the maximum of zonal wind. (c) Scatter plot including histograms of counts for the Principal component (PC) of the NPac-a mode versus the jet intensity (defined as max zonal wind). $R^2$ of linear fit and correlation coefficient are shown. For $E^{280}$ (black squares) and $Eoi^{280}$ (red diamonds). (d) Same, but for PC of NPac-z mode versus jet latitude (defined at latitude of max zonal wind).

where generally the northbound jet is stronger. The histogram of NPac-z PCs furthermore shows a negative skew, coinciding with this split jet or more northward jet in the $Eoi^{280}$. The $E^{280}$ distribution is slightly skewed towards positive NPac-z values, which implies a focused jet in the subtropics.

The temporal behavior of the jet as well as the correlation between the two NPac modes and the jet intensity and latitude suggest the following: In the $E^{280}$, the jet is mainly controlled by the NPac-a mode, with a high variation in jet intensity but not in latitude, while in the $Eoi^{280}$, the jet is mainly controlled by the NPac-z mode, with a high variation in the jet latitude and a tendency towards a strong northwards and weak southward jet, with less variation in jet intensity. The dominance of the NPac-a (NPac-z) in the $E^{280}$ ($Eoi^{280}$) corroborates our previous findings on the percentage of SLP variance explained by both modes (see Figure 6). A similar analysis using the global zonal mean zonal wind and the NHem mode is included in Supplementary material Figure S3.

### 3.3.2 The mid-Pliocene NPac-z mode

The state of the North Pacific jet stream in the NPac-z positive (PLUS) and negative (MIN) phases in the $E^{280}$ and $Eoi^{280}$ is shown in Figure 9, where the PLUS and MIN phases are defined as the ten average Januaries corresponding to the ten top and ten bottom NPac-z PC values, respectively. Figure 9 shows the zonal wind and 2PVU contour at 200 hPa on the right and the zonal mean between 160°E - 220°E on the left for both phases and the two simulations. The $E^{280}$ NPac-z MIN phase in Figure 9a shows a strong jet around 30°N that deflects southward, with a sharp 2PVU gradient along the jet core in the vertical in the central North Pacific. The $E^{280}$ NPac-z PLUS phase shown in Figure 9b shows a slightly weaker jet between 35 - 45°N, agreeing with a 2PVU gradient that is less sharp, that moves more northward over the North Pacific.

The $Eoi^{280}$ NPac-z MIN phase is shown in Figure 9c and shows similar zonal wind patterns and 2PVU contours as in the $E^{280}$, but at lower zonal winds (max 43.0 m/s in the central North Pacific zonal mean over 48.2 m/s in the $E^{280}$). The NPac-z PLUS phase in the $Eoi^{280}$ (Figure 9d) is different from the $E^{280}$, clearly showing the existence of two jets over the North Pacific, both on the 200 hPa isobar as well as in the vertical cross section. The northern jet (40.2 m/s, between 45-55°N) is stronger than the southern jet (27.2 m/s, between 15-25°N), confirming the suggestion of the existence of two jets based on the results in Figure 8d. The southern jet is located at lower pressures (or higher in the atmosphere) than the northern jet, although both jet cores follow the sharpest gradients of the 2PVU curve. The existence of this split jet over the North Pacific indicates a higher level of anticyclonic wave breaking on the northward side of the mean subtropical jet in comparison to the $E^{280}$, effectively deflecting the jet towards higher latitudes. The fact that in all cases the strongest jets are present where the meridional PV gradient is the strongest (see Figure 9 left panels) may indicate that the atmosphere is approximately in thermal wind balance in the January monthly mean. The nearly constant 2PVU height over latitude between the two jets in the $Eoi^{280}$ NPac-z PLUS (Figure 9d) furthermore indicates a high level of meridional mixing in the atmosphere between these two jets. The SAT, SIE and SLP anomalies associated with the NPac-z MIN and PLUS phases are shown in Supplementary Material Figure S4.

## 4 Discussion

### 4.1 Sensitivity to mid-Pliocene boundary conditions

In this study we have investigated mid-Pliocene Northern Hemisphere winter variability, and separated the response to either $CO_2$ or to mid-Pliocene boundary conditions other than $CO_2$. We find large differences between both climate forcings. In this section we want to explore which of the specific boundary condition changes in the $Eoi^{280}$, that include vegetation changes, closure of the Bering Strait and Canadian Arctic Archipelago (CAA), and minor topography differences (combined: “orography"), as well as a reduced Greenland Ice Sheet (GIS), can explain the observed response.

With the COSMOS coupled climate model, Stepanek et al. (2020) show that in the mid-Pliocene, just closing the Arctic gateways has a similar effect on springtime SIE than increasing $CO_2$ from 280 to 400 ppm. Using CCSM4 mid-Pliocene simulations, Otto-Bliesner et al. (2017) find that there is a similar response in North Pacific SIE to closing just the Bering Strait

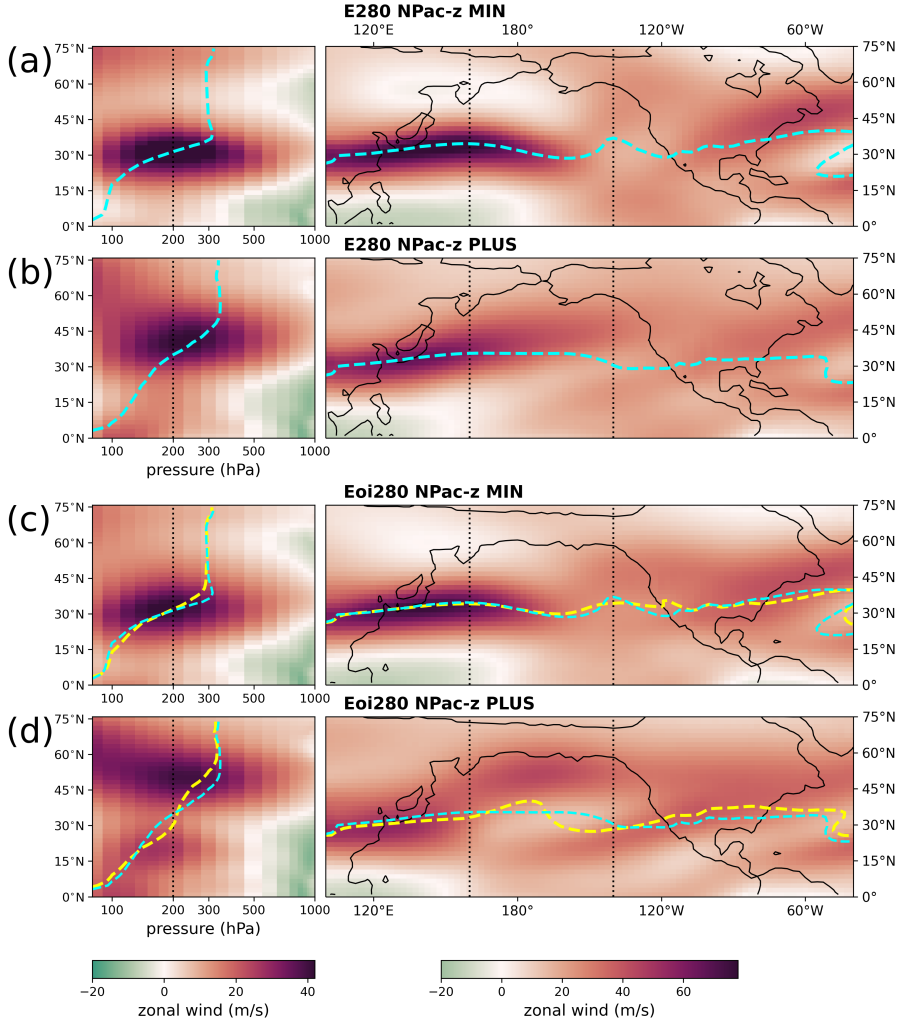


**Figure 9.** Zonal mean zonal wind between 160°E - 220°E (left) and zonal wind at 200 hPa (right). For the $E^{280}$ (a, b) and $Eoi^{280}$ (c, d), representing the NPac-z MIN phases (a, c) and PLUS phases (b, d). Dashed line indicates the 2PVU contour, in cyan for the $E^{280}$ and yellow for $Eoi^{280}$. Note that the colorbar range is slightly different for the left and right panels.

or just the CAA. Employing sensitivity studies with climate model CCSM4-UoT, Chandan and Peltier (2018) show that annual mean sea-ice volume in the Northern Hemisphere reduces most with implementation of mid-Pliocene orography, then with increased $CO_2$, and only then with the implementation of a reduced GIS. The annual mean SAT response to either changed orography or reduced GIS shows the largest response due to changed orography. They present the same SIE and SAT analysis for DJF in their Supplementary material, where the overall response is comparable to the annual mean findings.

Also using the CCSM4-UoT simulations, Menemenlis et al. (2021) find that a wintertime stationary wave pattern, present over the pre-industrial North Pacific and assessed via the eddy streamfunction, nearly disappears in the mid-Pliocene. They

show that this reduced wave train response is present in the simulations with only a different orography (and thus closed gateways), as well as the simulation with only a reduced GIS, but not in simulations with just elevated $CO_2$. They attribute the reduced wave train response to a reduced zonal SLP gradient and weakened jet stream over the North Pacific (similar findings to our $Eoi^{280}$ results), but do not explain why the changes in orography or GIS would cause these responses.

Considering results from those model studies, a larger response in annual and seasonal SAT and sea-ice due to changes in orography instead of changes in GIS would suggest that mainly the closed gateways are responsible for the changes in winter variability that we see in our own results. However, the sensitivity experiments with CCSM4-UoT indicate that both changes to orography as well as GIS have a similar effect on the wintertime dynamics over the North Pacific. All together, it makes it hard to draw a definite conclusion on which specific boundary conditions changes in the mid-Pliocene are responsible for the large differences between our $Eoi^{280}$ and $E^{280}$ results.

### 4.2 Physical and dynamical interpretation

Under $CO_2$ doubling, our simulations show a strengthened NPac-a mode, consistent with a general increase in SLP SD over the North Pacific. We also see a clear Arctic amplification response in the SAT, together with a large retreat of the winter SIE towards the pole. Simultaneously, there is a small increase in mean SLP and slight increase in STJ intensity over the North Pacific. The results are consistent with a study by Chen et al. (2018), that show a strengthening of PNA (or NPac-a) intensity under a strong future warming scenario in an ensemble of 35 CMIP5 models. They link it to a strengthening of the Aleutian low. A recent study by Simon et al. (2022) shows that winter sea-ice loss is associated with a deepening of the subpolar SLP low as well as a strengthening of the STJ, and connect that to a large positive PNA signal, all of which is consistent with our findings.

As a response to mid-Pliocene boundary conditions, we find a relative strengthening of the NPac-z mode and simultaneous weakening of the NPac-a mode, with a general decrease of SLP SD over the North Pacific. The NPac-z mode becomes dominant even on a hemispheric scale where it correlates strongly and significantly with the NHem mode. The North Pacific STJ becomes weaker (consistent with other PlioMIP2 studies; Hunter et al. (2019), Menemenlis et al. (2021) and Feng et al. (2022)) and more variable in latitude, which is correlated to NPac-z variability. The North Pacific winter climate is oscillating between states either with a relatively strong STJ, or with a split jet that has a strong northward jet and weak southward jet. In the winter mean, there is a strong increase in MSLP over the North Pacific, weakening the Aleutian low (consistent with Menemenlis et al., 2021). Simultaneously, there is a loss of winter sea ice connected to a warming in the northwest North Pacific, while a cooling is prominent over land that is now northwestern North America.

Menemenlis et al. (2021) find a similar SAT response in their mid-Pliocene simulations as our $Eoi^{280}$ response in Figure 3c and interpret it as a cool phase of the PDO, that is indeed connected to a weakened Aleutian low. However, we interpret the weakening of the Aleutian low in our simulation as a weakening of the dominance of the NPac-a mode (or PNA) in the pre-industrial, which simultaneously allows the NPac-z (or NPO) to exert more influence on the North Pacific winter climate. As Linkin and Nigam (2008) explain, the NPO can be considered a basin analogue to the NAO in the NAtl. In the present-day climate, the amplitude of the NAO is large and the NAtl jet relatively weak, while the NPO amplitude is small and the NPac jet

relatively strong. In our mid-Pliocene simulations, the NPac jet weakens up to 50% ánd the NPO becomes the dominant mode of variability in the NPac. This implies that - like the NAO in the present day NAtl - SLP anomalies related to NPO variability become successful in modulating the NPac jet. This is what we see in Figure 8d. The split jet condition over the NPac, related to the NPO PLUS phase in the mid-Pliocene simulation (Figure 9d), is also reminiscent of the dynamic behaviour of the jet in the present-day NAtl, corroborating the NAO analog even further.

In order to explain the large effect on the North Pacific winter variability (relative to North Atlantic) induced by mid-Pliocene boundary conditions, we identify three major aspects.

- **Surface temperatures:** Qualitatively, the SAT response to increased $CO_2$ and to the mid-Pliocene BCs is similar. However, Baatsen et al. (2022) show that for the CCSM4-Utr, the majority of the high-latitude $Eoi^{280}$ warming is due to a reduced planetary albedo, due to both reduced ice sheet and reduced sea-ice cover, while in the $E^{560}$ warming is mostly due to increased greenhouse gas concentrations (consistent with Chandan and Peltier (2018) and Burton et al. (2023)). Furthermore, the warming response to $CO_2$ is mostly zonally uniform with distinct Arctic amplification, while the response to mid-Pliocene BCs is more regional, especially over the North Pacific, where SAT increases over the western part and decreases over the eastern part. This typical warming pattern, referred to as a PDO cool phase in Menemenlis et al. (2021), is associated with a weakened Aleutian low and weakened STJ. According to Chen et al. (2018), a weakened Aleutian low means a weaker PNA, which is consistent with our findings. Hurwitz et al. (2012), employing sensitivity simulations, find that SST anomalies in the North Pacific reminiscent of our $Eoi^{280}$ warming pattern weaken the Aleutian low and in turn strengthen the NPO, which agrees with our findings. Most of the high latitude warming in the $Eoi^{280}$ is coming from orography changes rather than the reduced GIS (Chandan and Peltier, 2018). Hence, a surface warming pattern mainly caused by the closure of the Arctic gateways weakens the Aleutian low and allows the dominance of the NPO.

- **Atmospheric heat transport:** Mid-Pliocene simulations show a negative meridional heat transport anomaly in the mid- and high latitudes of the Northern Hemisphere, that is not caused by increased $CO_2$ (Chandan and Peltier, 2018; Baatsen et al., 2022; Burton et al., 2023). Chandan and Peltier (2018) show that this is largely caused by a significant reduction in Atmospheric Heat Transport (AHT) between 40-70°N, that is mainly the result of changes in orography and not changes to the GIS (nor of increased $CO_2$). Reduced AHT in the NHem is consistent with a weakening of the STJ, which strengthens the NPO (as described above). However, as we see in Figure 4, the zonal wind response is not the same for each latitude, and the STJ weakens greatly over the NPac, and shows little change over the NAtl. Reduced NHem annual mean AHT furthermore does not have to imply the same change in the winter season. Still, reduced AHT due to the changes in orography causes a weakened STJ, which favors the NPO.

- **Sea-ice changes:** We observe that the loss of winter sea ice is similar for the $Eoi^{280}$ as $E^{560}$ (Figure 3), where the North Pacific sea-ice loss in the mid-Pliocene is likely a response to the closed Arctic gateways (Otto-Bliesner et al., 2017; Chandan and Peltier, 2018). When considering present day sea-ice variations, the NPO strongly influences the marginal SIE variability in the Arctic (Linkin and Nigam, 2008) as well as in the Barents Sea (Xu and Fan, 2020). We find this

influence of the NPac-z on the marginal sea-ice zones in the Okhotsk, Bering and Barents Sea also in our $E^{280}$ and $Eoi^{280}$ simulation (see Figure S4). However, as SIE variability is largely driven by local atmospheric variability (Linkin and Nigam, 2008), it is more likely that changes in the NPac-z cause changes in Arctic SIE variability, instead of the other way around.

Finally, we address the nonlinearity and nonadditivity of the responses to changes in orography, GIS and $CO_2$. Garfinkel et al. (2020) use idealised models to find that the stationary wave response due to land-sea contrast (by means of surface albedo differences), due to heat fluxes in the ocean as well as due to topography, are nonlinear and non-additive. The nonadditivity is specifically important over the North Pacific, where they find that the response to these three forcings applied together is opposite from the sum of the responses of the three forcings applied in isolation. Our mid-Pliocene simulations see surface albedo changes due to changes in sea-ice cover and a reduced GIS, changes to heat fluxes in the ocean due to Arctic gateways being closed, ánd topography changes. Disentangling the relative effect of the mid-Pliocene BCs and increased $CO_2$, as we have done in this study, will therefore be difficult.

### 4.3 A climate variability point of view

How do the observed mid-Pliocene changes in North Pacific winter variability link to other modes of variability? Apart from the dominant Pacific teleconnection between canonical ENSO, PDO and PNA, the NPO has been linked to the North Pacific Meridional Mode (NPMM, Chiang and Vimont, 2004; Linkin and Nigam, 2008), as well as to the central Pacific El Niño, also known as El Niño Modoki or warm pool El Niño (Furtado et al., 2012; Ding et al., 2022). In the $Eoi^{280}$, we find reduced SLP variance in the North Pacific, with a relative weakening of the PNA and relative strengthening of the NPO. Furthermore, we know that in the $Eoi^{400}$ simulation with CCSM4-Utr the canonical El Niño variability reduces (Oldeman et al., 2021), as well as the variability of the PDO (Baatsen et al., 2022, referred to as Pacific Multidecadal Variability or PMV). The reduced canonical El Niño and PDO variability could explain the reduced PNA variability in the North Pacific winter. Oldeman et al. (2021) also show a slight relative increase in the number of central Pacific El Niño events over canonical El Niño events in the CCSM4-Utr $Eoi^{400}$, consistent with the relative strengthening of the NPO. However, the mid-Pliocene NPMM is shown to be a lot weaker in CCSM4-Utr compared to the pre-industrial by Pontes et al. (2022, extended data). Recently though, Stuecker (2018) showed that the PNA and PDO are also connected to the NPMM and central Pacific El Niño, especially on low frequencies. Our results consistently show a total reduction in the Pacific oceanic and atmospheric variability in the CCSM4-Utr mid-Pliocene simulations, with a clear reduction of the dominant teleconnection (being PNA, PDO and canonical Niño) and a relative increase of the prominence of the second leading teleconnection (being NPO, NPMM and central Pacific El Niño).

### 4.4 The mid-Pliocene as future climate analog?

In the Introduction, we posed the question whether the mid-Pliocene can be considered as an analog for future changes in atmospheric winter variability in the Northern Hemisphere. Burke et al. (2018) show that both following the RCP4.5 and

RCP8.5 scenarios, surface temperatures at the end of this century would be most analoguous to the mid-Pliocene. We find that the winter SAT and SIE response to $CO_2$ or to mid-Pliocene boundary conditions other than $CO_2$ are similar. This is consistent with Burton et al. (2023) that state that $CO_2$ is the dominant forcing in surface temperatures in the mid-Pliocene. However, we find that the response in winter SLP variability is almost opposite to both forcings, especially over the North Pacific. This is in a way 'consistent' with studies on the mid-Pliocene ENSO (Pontes et al., 2022) and AMOC (Weiffenbach et al., 2023), where the changes are opposite to end-of-the century projections. Feng et al. (2022) argue that the mid-Pliocene changes in ice sheets and vegetation are in some way a long-term Earth system feedback to elevated atmospheric $CO_2$. However, following the sensitivity study results in Chandan and Peltier (2018), it seems that the biggest influence on higher latitude climate are changes in orography, that is the closed Arctic gateways, rather than the reduced GIS. The Bering Strait is not expected to close in the coming centuries or millennia, so this disqualifies the mid-Pliocene as analogue for a future warm climate. However, the analysis in this paper is restricted explicitly to the Northern Hemisphere winter. Other seasons and regions in the world may behave differently, and potentially more analogous to what is expected for increased $CO_2$ levels.

## 5 Summary and conclusions

In this study, we address the question whether the mid-Pliocene climate can act as an analog for a future warm climate regarding Northern Hemisphere winter variability. We use a version of the CESM1.0.5, that is a part of PlioMIP2, and we show that the pre-industrial reference simulation is good in reproducing patterns of SLP variability, when compared to the CR20 reanalysis. We use a set of sensitivity simulations to separate the response to a $CO_2$ doubling and the response to mid-Pliocene boundary conditions other than $CO_2$.

We find that, although winter surface temperatures and sea-ice loss respond in a similar way to $CO_2$ or to mid-Pliocene boundary conditions, the response in mean SLP and jet stream show distinct differences. In the $CO_2$ doubling experiment, there is little response in mean SLP, while the mid-Pliocene shows a large increase in mean SLP over the North Pacific, together with a weakened jet stream. Regarding SLP variability, we find an increase in North Pacific SLP variance and a strengthening of the Pacific-North American pattern (PNA) in response to $CO_2$ doubling, consistent with literature, and no notable changes over the North Atlantic. An opposite response is seen in the mid-Pliocene boundary conditions simulation, where SLP variance decreases over the North Pacific, the PNA becomes weaker, and the North Pacific Oscillation (NPO) becomes the dominant mode of variability. We find a strong correlation between the PNA and North Pacific jet intensity on the one hand, and the NPO and jet latitude on the other hand, both in pre-industrial and mid-Pliocene climate. The pre-industrial climate, characterised by a strong PNA, shows a strong jet with variations in jet strength but not in latitude. The mid-Pliocene experiment shows a weak jet that is less variable in intensity, but has a high level of variation in jet latitude, consistent with a dominant NPO.

We suggest that the weakening of the Aleutian low, and subsequent relative dominance of the NPO over the PNA, is related to the typical surface temperature response in the mid-Pliocene. Although we do not have simulations that isolate the closed gateways and reduced Greenland Ice Sheet, based on other studies we suggest that this warming imprint is mostly an effect of the changes in orography, which includes the closure of the Bering Strait, rather than reduced Greenland Ice Sheet. Even

though the SAT response to $CO_2$ doubling looks qualitatively similar, the warming is more uniform over the North Pacific, and concentrates much more over the higher latitudes, whereas the mid-Pliocene warming is concentrated over the western North Pacific and shows a cool anomaly over the northeastern North Pacific. The opposite response in North Pacific winter variability to elevated $CO_2$ as opposed to mid-Pliocene boundary conditions weakens the notion of the mid-Pliocene climate as a future analog, especially since the closure of the Arctic gateways is not a long-term Earth system feedback to elevated $CO_2$.

Even though we consider the CESM1.0.5 a suitable model for this study, we might wonder whether every PlioMIP2 model shows the same response. In future research we plan to extend the investigation to the rest of the PlioMIP2 ensemble. In addition, the specific mechanisms by which the different mid-Pliocene boundary condition cause the changes in SLP variability and jet variations are not entirely clear. The specific response to these individual forcings, and the possible non-linear interaction between them, is an important open issue, which if resolved can help us understand how the winter climate responds to changing forcings in a warmer future.

*Code availability.* The Python scripts (Jupyter Notebooks) used for data analysis are freely accessible through Zenodo (https://doi.org/10.5281/zenodo.782 Oldeman (2023))

*Data availability.* Output from CCSM4-Utr simulations is available upon request. Please contact Michiel Baatsen (m.l.j.baatsen@uu.nl) for access. NOAA/CIRES/DOE 20th Century Reanalysis (V3) data is provided by the NOAA PSL, Boulder, Colorado, USA, from their website at https://psl.noaa.gov (last access: 28 February 2023). An evaluation of the performance of the CR20v3 can be found in Slivinski et al. (2021). Support for the Twentieth Century Reanalysis Project version 3 dataset is provided by the U.S. Department of Energy, Office of Science Biological and Environmental Research (BER), by the National Oceanic and Atmospheric Administration Climate Program Office, and by the NOAA Earth System Research Laboratory Physical Sciences Laboratory.

*Author contributions.* All authors contributed to the design of this work. AMO performed the analyses and wrote the manuscript.

*Competing interests.* The authors declare no competing interests.

*Acknowledgements.* The work was carried out under the program of the Netherlands Earth System Science Centre (NESSC), financially supported by the Ministry of Education, Culture and Science (OCW grant number 024.002.001). Simulations were performed at the SURFsara Dutch national computing facilities and were sponsored by NWO-EW (Netherlands Organisation for Scientific Research, Exact Sciences) (project nos. 17189 and 2020.022). The authors would like to thank Michael Kliphuis for setting up and managing the CCSM4-Utr model simulations, and Ezekiel Djeribi Stevens for their performed analysis and interpretation on the CCSM4-Utr NAO.

## References


Abell, J. T., Winckler, G., Anderson, R. F., and Herbert, T. D.: Poleward and weakened westerlies during Pliocene warmth, Nature, 589, 70–75, https://doi.org/10.1038/s41586-020-03062-1, 2021.

Ambaum, M. H., Hoskins, B. J., and Stephenson, D. B.: Arctic Oscillation or North Atlantic Oscillation?, Journal of Climate, 14, 3495–3507, https://doi.org/10.1175/1520-0442(2001)014<3495:AOONAO>2.0.CO;2, 2001.

Baatsen, M. L. J., von der Heydt, A. S., Kliphuis, M. A., Oldeman, A. M., and Weiffenbach, J. E.: Warm mid-Pliocene conditions without high climate sensitivity: the CCSM4-Utrecht (CESM 1.0.5) contribution to the PlioMIP2, Climate of the Past, 18, 657–679, https://doi.org/10.5194/cp-18-657-2022, 2022.

Barnston, A. G. and Livezey, R. E.: Classification, Seasonality and Persistence of Low-Frequency Atmospheric Circulation Patterns, Monthly Weather Review, 115, 1083–1126, https://doi.org/10.1175/1520-0493(1987)115<1083:CSAPOL>2.0.CO;2, 1987.

Behera, P., Tiwari, M., Kumar, V., Sarathchandraprasad, T., and Tripathi, S.: South Asian Monsoon Variability and Arctic Sea Ice Extent Linkages During the Late Pliocene, Paleoceanography and Paleoclimatology, 37, https://doi.org/10.1029/2022PA004436, 2022.

Blackport, R. and Fyfe, J. C.: Climate models fail to capture strengthening wintertime North Atlantic jet and impacts on Europe, Science Advances, 8, https://doi.org/10.1126/sciadv.abn3112, 2022.

Burke, K. D., Williams, J. W., Chandler, M. A., Haywood, A. M., Lunt, D. J., and Otto-Bliesner, B. L.: Pliocene and Eocene provide best analogs for near-future climates, Proceedings of the National Academy of Sciences of the United States of America, 115, 13 288–13 293, https://doi.org/10.1073/pnas.1809600115, 2018.

Burton, L. E., Haywood, A. M., Tindall, J. C., Dolan, A. M., Hill, D. J., Abe-Ouchi, A., Chan, W.-L., Chandan, D., Feng, R., Hunter, S. J., Li, X., Peltier, W. R., Tan, N., Stepanek, C., and Zhang, Z.: On the climatic influence of $CO_2$ forcing in the Pliocene, Climate of the Past, 19, 747–764, https://doi.org/10.5194/cp-19-747-2023, 2023.

Chandan, D. and Peltier, W. R.: On the mechanisms of warming the mid-Pliocene and the inference of a hierarchy of climate sensitivities with relevance to the understanding of climate futures, Climate of the Past, 14, 825–856, https://doi.org/10.5194/cp-14-825-2018, 2018.

Chen, D., Rojas, M., Samset, B., Cobb, K., Diongue Niang, A., Edwards, P., Emori, S., Faria, S., Hawkins, E., Hope, P., Huybrechts, P., Meinshausen, M., Mustafa, S., Plattner, G.-K., and Tréguier, A.-M.: Framing, Context, and Methods (Chapter 1), in: Climate Change 2021: The Physical Science Basis. Contribution of Working Group I to the Sixth Assessment Report of the Intergovernmental Panel on Climate Change, pp. 147–286, Cambridge University Press, doi: 10.1017/9781009157896.003, 2021.

Chen, Z., Gan, B., Wu, L., and Jia, F.: Pacific-North American teleconnection and North Pacific Oscillation: historical simulation and future projection in CMIP5 models, Climate Dynamics, 50, 4379–4403, https://doi.org/10.1007/s00382-017-3881-9, 2018.

Chiang, J. C. H. and Vimont, D. J.: Analogous Pacific and Atlantic Meridional Modes of Tropical Atmosphere–Ocean Variability, Journal of Climate, 17, 4143–4158, https://doi.org/10.1175/JCLI4953.1, 2004.

De Nooijer, W., Zhang, Q., Li, Q., Zhang, Q., Li, X., Zhang, Z., Guo, C., Nisancioglu, K. H., Haywood, A. M., Tindall, J. C., Hunter, S. J., Dowsett, H. J., Stepanek, C., Lohmann, G., Otto-Bliesner, B. L., Feng, R., Sohl, L. E., Chandler, M. A., Tan, N., Contoux, C., Ramstein, G., Baatsen, M. L., Von Der Heydt, A. S., Chandan, D., Peltier, W. R., Abe-Ouchi, A., Chan, W. L., Kamae, Y., and Brierley, C. M.: Evaluation of Arctic warming in mid-Pliocene climate simulations, Climate of the Past, 16, 2325–2341, https://doi.org/10.5194/cp-16-2325-2020, 2020.

Deser, C., Hurrell, J. W., and Phillips, A. S.: The role of the North Atlantic Oscillation in European climate projections, Climate Dynamics, 49, 3141–3157, https://doi.org/10.1007/s00382-016-3502-z, 2017.

Ding, R., Tseng, Y., Di Lorenzo, E., Shi, L., Li, J., Yu, J.-Y., Wang, C., Sun, C., Luo, J.-J., Ha, K., Hu, Z.-Z., and Li, F.: Multi-year El Niño events tied to the North Pacific Oscillation, Nature Communications, 13:3871, https://doi.org/10.1038/s41467-022-31516-9, 2022.

Dowsett, H., Dolan, A., Rowley, D., Moucha, R., Forte, A. M., Mitrovica, J. X., Pound, M., Salzmann, U., Robinson, M., Chandler, M., Foley, K., and Haywood, A.: The PRISM4 (mid-Piacenzian) paleoenvironmental reconstruction, Climate of the Past, 12, 1519–1538, https://doi.org/10.5194/cp-12-1519-2016, 2016.

Eyring, V., Gillet, N., Achuta Rao, K., Barimalala, R., Barreiro Parrillo, M., Bellouin, N., Cassou, C., Durack, P., Kosaka, Y., McGregor, S., Min, S., Morgenstern, O., and Sun, Y.: Human Influence on the Climate System (Chapter 3), in: Climate Change 2021: The Physical Science Basis. Contribution of Working Group I to the Sixth Assessment Report of the Intergovernmental Panel on Climate Change, pp. 423–552, Cambridge University Press, doi: 10.1017/9781009157896.005, 2021.

Feng, R., Bhattacharya, T., Otto-Bliesner, B. L., Brady, E. C., Haywood, A. M., Tindall, J. C., Hunter, S. J., Abe-Ouchi, A., Chan, W.-L., Kageyama, M., Contoux, C., Guo, C., Li, X., Lohmann, G., Stepanek, C., Tan, N., Zhang, Q., Zhang, Z., Han, Z., Williams, C. J. R., Lunt, D. J., Dowsett, H. J., Chandan, D., and Peltier, W. R.: Past terrestrial hydroclimate sensitivity controlled by Earth system feedbacks, Nature Communications, 13:1306, 1306, https://doi.org/10.1038/s41467-022-28814-7, 2022.

Fereday, D., Chadwick, R., Knight, J., and Scaife, A. A.: Atmospheric Dynamics is the Largest Source of Uncertainty in Future Winter European Rainfall, Journal of Climate, 31, 963–977, https://doi.org/10.1175/JCLI-D-17-0048.1, 2018.

Furtado, J. C., Di Lorenzo, E., Anderson, B. T., and Schneider, N.: Linkages between the North Pacific Oscillation and central tropical Pacific SSTs at low frequencies, Climate Dynamics, 39, 2833–2846, https://doi.org/10.1007/s00382-011-1245-4, 2012.

Garfinkel, C. I., White, I., Gerber, E. P., Jucker, M., and Erez, M.: The Building Blocks of Northern Hemisphere Wintertime Stationary Waves, Journal of Climate, 33, 5611–5633, https://doi.org/10.1175/JCLI-D-19-0181.1, 2020.

Han, Z., Zhang, Q., Li, Q., Feng, R., Haywood, A. M., Tindall, J. C., Hunter, S. J., Otto-Bliesner, B. L., Brady, E. C., Rosenbloom, N., Zhang, Z., Li, X., Guo, C., Nisancioglu, K. H., Stepanek, C., Lohmann, G., Sohl, L. E., Chandler, M. A., Tan, N., Ramstein, G., Baatsen, M. L. J., von der Heydt, A. S., Chandan, D., Peltier, W. R., Williams, C. J. R., Lunt, D. J., Cheng, J., Wen, Q., and Burls, N. J.: Evaluating the large-scale hydrological cycle response within the Pliocene Model Intercomparison Project Phase 2 (PlioMIP2) ensemble, Climate of the Past, 17, 2537–2558, https://doi.org/10.5194/cp-17-2537-2021, 2021.

Haywood, A., Tindall, J., Dowsett, H., Dolan, A., Foley, K., Hunter, S., Hill, D., Chan, W.-L., Abe-Ouchi, A., Stepanek, C., Lohmann, G., Chandan, D., Peltier, W. R., Tan, N., Contoux, C., Ramstein, G., Li, X., Zhang, Z., Guo, C., Nisancioglu, K., Zhang, Q., Li, Q., Kamae, Y., Chandler, M., Sohl, L., Otto-Bliesner, B., Feng, R., Brady, E., von der Heydt, A., Baatsen, M., and Lunt, D.: The Pliocene Model Intercomparison Project Phase 2: large-scale climate features and climate sensitivity, Climate of The Past, 16,, 2095–2123, https://doi.org/10.5194/cp-2019-145, 2020.

Haywood, A. M., Dowsett, H. J., Dolan, A. M., Rowley, D., Abe-Ouchi, A., Otto-Bliesner, B., Chandler, M. A., Hunter, S. J., Lunt, D. J., Pound, M., and Salzmann, U.: The Pliocene Model Intercomparison Project (PlioMIP) Phase 2: Scientific objectives and experimental design, Climate of the Past, 12, 663–675, https://doi.org/10.5194/cp-12-663-2016, 2016.

Hill, D. J., Csank, A. Z., Dolan, A. M., and Lunt, D. J.: Pliocene climate variability: Northern Annular Mode in models and tree-ring data, Palaeogeography, Palaeoclimatology, Palaeoecology, 309, 118–127, https://doi.org/10.1016/j.palaeo.2011.04.003, 2011.

Hunter, S. J., Haywood, A. M., Dolan, A. M., and Tindall, J. C.: The HadCM3 contribution to PlioMIP phase 2, Climate of the Past, 15, 1691–1713, https://doi.org/10.5194/cp-15-1691-2019, 2019.

Hurrell, J. W. and Deser, C.: North Atlantic climate variability: The role of the North Atlantic Oscillation, Journal of Marine Systems, 79, 231–244, https://doi.org/10.1016/j.jmarsys.2009.11.002, 2010.

Hurwitz, M. M., Newman, P. A., and Garfinkel, C. I.: On the influence of North Pacific sea surface temperature on the Arctic winter climate, Journal of Geophysical Research, 117, https://doi.org/10.1029/2012JD017819, 2012.

Iles, C. and Hegerl, G.: Role of the North Atlantic Oscillation in decadal temperature trends, Environmental Research Letters, 12, 114 010, https://doi.org/10.1088/1748-9326/aa9152, 2017.

Kunz, A., Konopka, P., Müller, R., and Pan, L. L.: Dynamical tropopause based on isentropic potential vorticity gradients, Journal of Geophysical Research, 116, https://doi.org/10.1029/2010JD014343, 2011.

Linkin, M. E. and Nigam, S.: The North Pacific Oscillation-West Pacific teleconnection pattern: Mature-phase structure and winter impacts, Journal of Climate, 21, 1979–1997, https://doi.org/10.1175/2007JCLI2048.1, 2008.

Menemenlis, S., Lora, J. M., Lofverstrom, M., and Chandan, D.: Influence of stationary waves on mid-Pliocene atmospheric rivers and hydroclimate, Global and Planetary Change, 204, https://doi.org/10.1016/j.gloplacha.2021.103557, 2021.

Oldeman, A. M.: Zenodo codes, arthuroldeman/midpliocene-nam v1.0, https://doi.org/10.5281/zenodo.7825540, 2023.

Oldeman, A. M., Baatsen, M. L. J., von der Heydt, A. S., Dijkstra, H. A., Tindall, J. C., Abe-Ouchi, A., Booth, A. R., Brady, E. C., Chan, W.-L., Chandan, D., Chandler, M. A., Contoux, C., Feng, R., Guo, C., Haywood, A. M., Hunter, S. J., Kamae, Y., Li, Q., Li, X., Lohmann, G., Lunt, D. J., Nisancioglu, K. H., Otto-Bliesner, B. L., Peltier, W. R., Pontes, G. M., Ramstein, G., Sohl, L. E., Stepanek, C., Tan, N., Zhang, Q., Zhang, Z., Wainer, I., and Williams, C. J. R.: Reduced El Niño variability in the mid-Pliocene according to the PlioMIP2 ensemble, Climate of the Past, 17, 2427–2450, https://doi.org/10.5194/cp-17-2427-2021, 2021.

Osborn, T. J.: Simulating the winter North Atlantic Oscillation: the roles of internal variability and greenhouse gas forcing, Climate Dynamics, 22, 605–623, https://doi.org/10.1007/s00382-004-0405-1, 2004.

Otto-Bliesner, B. L., Jahn, A., Feng, R., Brady, E. C., Hu, A., and Löfverström, M.: Amplified North Atlantic warming in the late Pliocene by changes in Arctic gateways, Geophysical Research Letters, 44, 957–964, https://doi.org/10.1002/2016GL071805, 2017.

Pontes, G. M., Taschetto, A. S., Sen Gupta, A., Santoso, A., Wainer, I., Haywood, A. M., Chan, W.-L., Abe-Ouchi, A., Stepanek, C., Lohmann, G., Hunter, S. J., Tindall, J. C., Chandler, M. A., Sohl, L. E., Peltier, W. R., Chandan, D., Kamae, Y., Nisancioglu, K. H., Zhang, Z., Contoux, C., Tan, N., Zhang, Q., Otto-Bliesner, B. L., Brady, E. C., Feng, R., von der Heydt, A. S., Baatsen, M. L. J., and Oldeman, A. M.: Mid-Pliocene El Niño/Southern Oscillation suppressed by Pacific intertropical convergence zone shift, Nature Geoscience, 15, 726–734, https://doi.org/10.1038/s41561-022-00999-y, 2022.

Shepherd, T. G.: Atmospheric circulation as a source of uncertainty in climate change projections, Nature Geoscience, 7, 703–708, https://doi.org/10.1038/ngeo2253, 2014.

Simon, A., Gastineau, G., Frankignoul, C., Lapin, V., and Ortega, P.: Pacific Decadal Oscillation modulates the Arctic sea-ice loss influence on the midlatitude atmospheric circulation in winter, Weather and Climate Dynamics, 3, 17, 2022.

Slivinski, L. C., Compo, G. P., Sardeshmukh, P. D., Whitaker, J. S., McColl, C., Allan, R. J., Brohan, P., Yin, X., Smith, C. A., Spencer, L. J., Vose, R. S., Rohrer, M., Conroy, R. P., Schuster, D. C., Kennedy, J. J., Ashcroft, L., Brönnimann, S., Brunet, M., Camuffo, D., Cornes, R., Cram, T. A., Domínguez-Castro, F., Freeman, J. E., Gergis, J., Hawkins, E., Jones, P. D., Kubota, H., Lee, T. C., Lorrey, A. M., Luterbacher, J., Mock, C. J., Przybylak, R. K., Pudmenzky, C., Slonosky, V. C., Tinz, B., Trewin, B., Wang, X. L., Wilkinson, C., Wood, K., and Wyszyński, P.: An Evaluation of the Performance of the Twentieth Century Reanalysis Version 3, Journal of Climate, 34, 1417–1438, https://doi.org/10.1175/JCLI-D-20-0505.1, 2021.

Stepanek, C., Samakinwa, E., Knorr, G., and Lohmann, G.: Contribution of the coupled atmosphere–ocean–sea ice–vegetation model COSMOS to the PlioMIP2, Climate of the Past, 16, 2275–2323, https://doi.org/10.5194/cp-16-2275-2020, 2020.

Stuecker, M. F.: Revisiting the Pacific Meridional Mode, Scientific Reports, 8:3216, https://doi.org/10.1038/s41598-018-21537-0, 2018.

Tindall, J. C., Haywood, A. M., Salzmann, U., Dolan, A. M., and Fletcher, T.: The warm winter paradox in the Pliocene northern high latitudes, Climate of the Past, 18, 1385–1405, https://doi.org/10.5194/cp-18-1385-2022, 2022.

Weiffenbach, J. E., Baatsen, M. L. J., Dijkstra, H. A., von der Heydt, A. S., Abe-Ouchi, A., Brady, E. C., Chan, W.-L., Chandan, D., Chandler, M. A., Contoux, C., Feng, R., Guo, C., Han, Z., Haywood, A. M., Li, Q., Li, X., Lohmann, G., Lunt, D. J., Nisancioglu, K. H., Otto-Bliesner, B. L., Peltier, W. R., Ramstein, G., Sohl, L. E., Stepanek, C., Tan, N., Tindall, J. C., Williams, C. J. R., Zhang, Q., and Zhang, Z.: Unraveling the mechanisms and implications of a stronger mid-Pliocene Atlantic Meridional Overturning Circulation (AMOC) in PlioMIP2, Climate of the Past, 19, 61–85, https://doi.org/10.5194/cp-19-61-2023, 2023.

Woollings, T.: Dynamical influences on European climate: an uncertain future, Philosophical Transactions of the Royal Society A: Mathematical, Physical and Engineering Sciences, 368, 3733–3756, https://doi.org/10.1098/rsta.2010.0040, 2010.

Xu, Z. and Fan, K.: Prolonged Periodicity and Eastward Shift of the January North Pacific Oscillation Since the Mid-1990s and Its Linkage With Sea Ice Anomalies in the Barents Sea, Journal of Geophysical Research: Atmospheres, 125, https://doi.org/10.1029/2020JD032484, 2020.

Zhang, Z., Li, X., Guo, C., Otterå, O. H., Nisancioglu, K., Tan, N., Contoux, C., Ramstein, G., Feng, R., Otto-Bliesner, B., Brady, E., Chandan, D., Peltier, W. R., Baatsen, M., von der Heydt, A., Weiffenbach, J., Stepanek, C., Lohmann, G., Zhang, Q., Li, Q., Chandler, M., Sohl, L., Haywood, A., Hunter, S., Tindall, J., Williams, C., Lunt, D., Chan, W.-L., and Abe-Ouchi, A.: Mid-Pliocene Atlantic Meridional Overturning Circulation simulated in PlioMIP2, Climate of the Past, 17, 529–543, https://doi.org/10.5194/cp-2020-120, 2020.